which case some of the symptoms could reflect molybdenum insufficiency. Finally, activation or aggregation of GlyRs might modulate the ability of gephyrin to promote molybdopterin biosynthesis, thus resulting in a functional link between molybdoenzymes and inhibitory neurotransmission.

References and Notes

1. M. H. Aprison, in *Glycine Neurotransmission*, O. P. Ottoson and J. Storm-Mathisen, Eds. (Wiley, New York, 1990), pp. 1–24; P. Jonas, J. Bischofberger, J. Sandkühler, *Science* **281**, 419 (1998).
2. F. Pfeiffer, D. Graham, H. Betz, *J. Biol. Chem.* **257**, 9389 (1982).
3. G. Meyer, J. Kirsch, H. Betz, D. Langosch, *Neuron* **15**, 563 (1995); J. Kirsch *et al.*, *J. Biol. Chem.* **266**, 22242 (1991); J. Kirsch and H. Betz, *J. Neurosci.* **15**, 4148 (1995).
4. A. Triller, F. Cluzeaud, F. Pfeiffer, H. Betz, H. Korn, *J. Cell Biol.* **101**, 683 (1985); J. Kirsch and H. Betz, *Brain Res.* **621**, 301 (1993); A. J. Todd, R. C. Spike, D. Chong, M. Neilson, *Eur. J. Neurosci.* **7**, 1 (1995).
5. J. Kirsch, J. Kuhse, H. Betz, *Mol. Cell. Neurosci.* **6**, 450 (1995); J. Kirsch, I. Wolters, A. Triller, H. Betz, *Nature* **366**, 745 (1993).
6. J. Kirsch, G. Meyer, H. Betz, *Mol. Cell. Neurosci.* **8**, 93 (1996); C. Bechade and A. Triller, *Semin. Cell Dev. Biol.* **7**, 717 (1996).
7. P. Prior *et al.*, *Neuron* **8**, 1161 (1992).
8. K. V. Rajagopalan, *Biochem. Soc. Trans.* **25**, 757 (1997); K. P. Kamdar *et al.*, *ibid.*, p. 778; B. Stallmeyer, A. Nerlich, J. Schiemann, H. Brinkmann, R. R. Mendel, *Plant J.* **8**, 751 (1995).
9. M. Ramming, H. Betz, J. Kirsch, *FEBS Lett.* **405**, 137 (1997).
10. The targeting vector contained a 5-kb Eco RI/Sac I genomic fragment in which a phosphoglycerate kinase–neo cassette replaced a Pst I/Eag I fragment that encoded the putative promoter region of the murine gephyrin gene as well as the first exon, which included the initiator methionine (*9*). The construct was transfected into R1 ES cells [A. Nagy, J. Rossant, R. Nagy, W. Abramow-Newerly, J. C. Roder, *Proc. Natl. Acad. Sci. U.S.A.* **90**, 8424 (1993)], and 20 of 200 clones screened were identified as homologous recombinants. Homozygotes derived from two independently derived ES cell clones showed identical phenotypes. For Southern (DNA) analysis, a 0.6-kb probe external to the short arm (Fig. 1B) was hybridized to Eco RV–digested genomic DNA. For Northern analysis, 10-μg aliquots of polyadenylated RNA from brain were separated in a 1% agarose gel, and a blot was probed successively with cDNAs encoding mouse gephyrin, sulfite oxidase, or GlyR α1 subunit. For Western analysis, brain protein extracts were fractionated on 6% or 10% SDS polyacrylamide gels, and immunoblots were probed with mouse monoclonal antibodies directed against the COOH-terminus of gephyrin (Transduction Labs) or GlyR subunits [monoclonal antibody (mAb) 4a; (*24*)].
11. Spinal cords and brains were cross-sectioned at 7 μm in a cryostat. Sections were fixed with 4% paraformaldehyde and stained with antibodies specific for GlyR α1 subunit [mAb 2b; (*24*)], gephyrin [mAbs 5a and 7a; (*24*)], SV2 (gift of K. Buckley, Harvard University), the PSD-95/SAP-90 family (Upstate Biotechnology), the glutamate receptor GluR1 subunit (Upstate Biotechnology), or synaptophysin (gift of A. Czernik, Rockefeller University). Other sections were stained with hematoxylin and eosin.
12. M. Sheng and M. Wyszynski, *Bioessays* **19**, 847 (1997).
13. E. S. Simon, *Mov. Disord.* **12**, 221 (1997).
14. J. L. Johnson and S. K. Wadman, in *The Metabolic Basis of Inherited Diseases*, C. R. Scrivner, A. L. Beaudef, W. S. Sly, D. Valle, Eds. (McGraw-Hill, New York, 1995), pp. 2271–2283
15. For sulfite oxidase assay, livers were homogenized and centrifuged at 16,000*g* for 20 min. Supernatants were desalted on Sephadex G-25 (Pharmacia). Activity in the flow-through was determined as described [J. L. Johnson *et al.*, *J. Inherit. Metab. Dis.* **14**, 932 (1991)].
16. M. Nakamura and I. Yamazaki, *J. Biochem.* **92**, 1279 (1972).
17. Xanthine dehydrogenase assay was modified from D. A. Parks, T. K. Williams, and J. S. Beckman [*Am. J. Physiol.* **254** 768 (1988)]. Intestines were homogenized in 50 mM potassium phosphate (pH 7.0), 10 mM dithiothreitol, 1 mM phenylmethylsulfonyl fluoride, and 0.1 mM EDTA. After centrifugation at 16,000*g* for 20 min, 200-μl aliquots of supernatant were incubated with 100 μl of 500 μM nicotinamide adenine dinucleotide, 100 μl of 50 μM xanthine, and 600 μl of 50 mM potassium phosphate (pH 7.8). Formation of uric acid from xanthine was monitored at 295 nm wavelength in the presence or absence of 5 μM allopurinol, an inhibitor of xanthine dehydrogenase [R. W. E. Watts, J. E. M. Watts, J. E. Seegmiller, *J. Lab. Clin. Med.* **66**, 688 (1965)].
18. Lactate dehydrogenase activity was determined as described [A. Yoshida and E. Freese, *Methods Enzymol.* **41**, 304 (1975)]. Protein was assayed with the Bradford reagent (Bio-Rad).
19. C. A. Rupar *et al.*, *Neuropediatrics* **27**, 299 (1996).
20. H. Nishimaru, M. Iizuka, S. Ozaki, N. Kudo, *J. Physiol. (London)* **497**, 131 (1996).
21. W.-L. Wu, L. Ziskind-Conhaim, M. A. Sweet, *J. Neurosci.* **12**, 3935 (1992).
22. M. Gautam *et al.*, *Nature* **377**, 232 (1995); M. Gautum *et al.*, *Cell* **85**, 525 (1996); T. M. DeChiara *et al.*, *ibid.*, p. 501; J. R. Sanes and J. W. Lichtman, *Annu. Rev. Neurosci.*, in press.
23. W. Brune *et al.*, *Am. J. Hum. Genet.* **58**, 959 (1996); M. Andrew and M. J. Owen, *Br. J. Psychiatry* **170**, 106 (1997).
24. F. Pfeiffer, R. Simler, G. Grenningloh, H. Betz, *Proc. Natl. Acad. Sci. U.S.A.* **81**, 7224 (1984).

25. Supported by grants from NIH (J.R.S.), the Jane Coffin Childs Memorial Fund for Medical Research (G.F.), the McKnight Foundation (J.R.S.) the Deutsche Forschungsgemeinschaft, BMBF, and Fonds der Chemischen Industrie (H.B.). We thank I. Bartuik, C. Borgmeyer, J. Cunningham, J. Gross, and S. Weng for assistance. We dedicate this paper to the memory of Rolf Westkamp.

20 August 1998; accepted 25 September 1998

Structure of Human Methionine Aminopeptidase-2 Complexed with Fumagillin

Shenping Liu, Joanne Widom, Christopher W. Kemp, Craig M. Crews, Jon Clardy*

The fungal metabolite fumagillin suppresses the formation of new blood vessels, and a fumagillin analog is currently in clinical trials as an anticancer agent. The molecular target of fumagillin is methionine aminopeptidase-2 (MetAP-2). A 1.8 Å resolution crystal structure of free and inhibited human MetAP-2 shows a covalent bond formed between a reactive epoxide of fumagillin and histidine-231 in the active site of MetAP-2. Extensive hydrophobic and water-mediated polar interactions with other parts of fumagillin provide additional affinity. Fumagillin-based drugs inhibit MetAP-2 but not MetAP-1, and the three-dimensional structure also indicates the likely determinants of this specificity. The structural basis for fumagillin's potency and specificity forms the starting point for structure-based drug design.

Angiogenesis, the growth of new blood vessels, is a pathological determinant in tumor progression, diabetic retinopathy, and rheumatoid arthritis (*1*). The serendipitous discovery that fumagillin, a fungal metabolite, potently inhibits angiogenesis initiated the systematic development of small molecule angiogenesis inhibitors (*2, 3*) (Fig. 1). One semisynthetic derivative of fumagillin, TNP-470, is in clinical trials as an anticancer agent (Fig. 1) (*3, 4*). Fumagillin-based affinity reagents identified MetAP-2 as the specific cellular target of fumagillin, and this specificity was confirmed with genetically altered yeast strains (*5, 6*). The correlation between the antiproliferative activity of several fumagillin analogs with their ability to inhibit MetAP-2 activity in vitro suggests that MetAP-2 is the physiologically relevant target of fumagillin-based therapeutic agents (*6*). This suggestion is strengthened by a recent report that human endothelial cells are especially sensitive to fumagillin and that proliferation of these cells can be blocked by human MetAP-2 antisense oligonucleotides (*7*). MetAPs, which

S. Liu, J. Widom, J. Clardy, Department of Chemistry and Chemical Biology, Baker Laboratory, Cornell University, Ithaca, NY 14853–1301, USA. C. W. Kemp, Kemp Biotechnologies, Incorporated, Frederick, MD 21704, USA. C. M. Crews, Department of Molecular, Cellular, and Developmental Biology, Kline Biology Tower, Yale University, New Haven, CT 06520–8103, USA.

*To whom correspondence should be addressed. E-mail: jcc12@cornell.edu

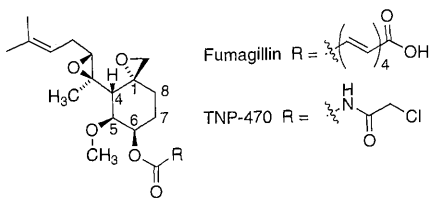

Fig. 1. The chemical structure of fumagillin and TNP-470.

remove NH_2-terminal methionines from proteins in a nonprocessive manner, are highly conserved in sequence (*8*) (Fig. 2). These cobalt-containing metalloproteases are divided into two families, type 1 (MetAP-1) and type 2 (MetAP-2), and fumagillin inhibits the in vivo activity of only MetAP-2 (*5, 6*).

To investigate fumagillin's inhibitory mechanism, we determined the crystal structure of human MetAP-2 with and without bound fumagillin. Human MetAP-2 (HsMetAP-2) was expressed in Sf21 insect cells (*9*). Crystals of HsMetAP-2 were prepared, diffraction data were collected at the F1 station of CHESS, and the structure was solved by the molecular replacement method (*10, 11*). The structure has been refined to a final *R* factor of 0.183 and 0.194 for native and fumagillin-complexed HsMetAP-2, respectively, for the 1.8 to 25.0 Å data (Fig. 3A) (*11*).

Earlier crystallographic studies of the MetAP-1 from *Escherichia coli* (EcMetAP-1) (*12*) and the MetAP-2 from *Pyrococcus furiosus* (PfMetAP-2) (*13*) have defined the overall topology of the MetAP family. Like EcMetAP-1 and PfMetAP-2, HsMetAP-2 has a central β sheet with an active site located roughly at the center of the sheet's concave face (Fig. 3B). Two pairs of α helices (α1-α2, α3-α4) and a short COOH-terminal tail cover the sheet's convex face (Fig. 3B).

HsMetAP-2 has several features that distinguish it from the prokaryotic MetAPs (Fig. 2). HsMetAP-2, unlike EcMetAP-1 and PfMetAP-2, has a 165-residue NH_2-terminal extension, which is not essential for aminopeptidase activity (*6*). In the structure described here, the NH_2-terminal extension is largely disordered, and clear electron density begins at Lys^{110} with a disordered loop from residues 138 to 153 (Fig. 3B). The visible portion of the NH_2-terminal extension lies on the convex surface near helices α1 and α2 and far from the active site.

Residues 381 to 444, the long insertion that distinguishes the MetAP-2 family from the MetAP-1 family (Fig. 2), comprise the end of β7, α5, α6, α7, and the beginning of β8 and form a compact domain that does not interact significantly with the rest of the protein (Fig. 3B). A small insertion, which includes β4 and the beginning of β5 (residues 312 to 319), distinguishes eukaryotic from prokaryotic MetAP-2. Neither of these insertions disrupts the MetAP-1 secondary structure (Figs. 2 and 3B). The insertions and NH_2-terminal extension in HsMetAP-2 break the pseudo twofold symmetry of EcMetAP-1 (*12*).

The active site is a deep pocket with two cobalts at its base and a completely covered side pocket that presumably serves as the specificity pocket for the NH_2-terminal methionine side chain of natural substrates. Reorientation of the Tyr^{444} side chain and some water molecules opens this pocket to solvent. The Tyr^{444} residue is completely conserved in the

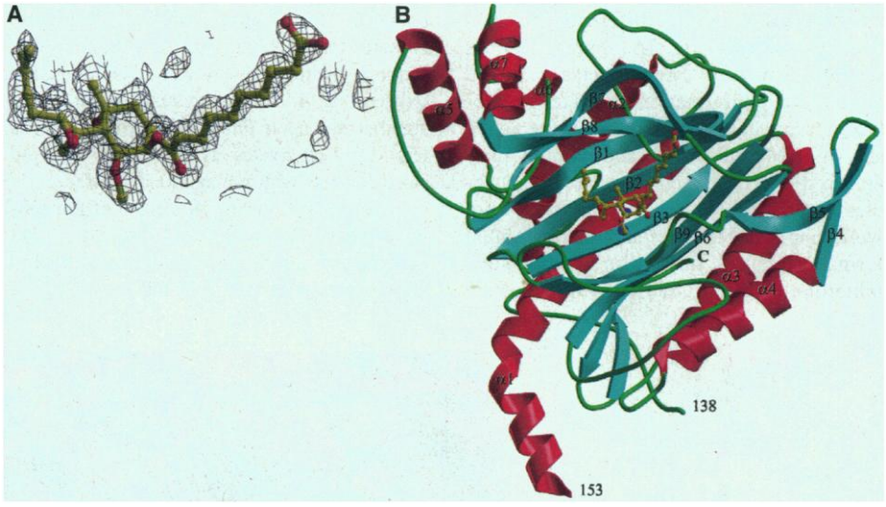

Fig. 3. (**A**) Electron density ($|F_{complex} - F_{native}|$, native phases, 3σ contour level) of fumagillin in the catalytic pocket of human MetAP-2. An atomic model of the final structure is embedded in this electron density. (**B**) Overall structure of the complex between human MetAP-2 (red, green, and blue) and fumagillin (yellow and red ball and stick). The two metals at the catalytic site are dark blue spheres partly obscured by fumagillin. Secondary structural elements of MetAP-2 are labeled. Drawing prepared with Molscript (*18*).

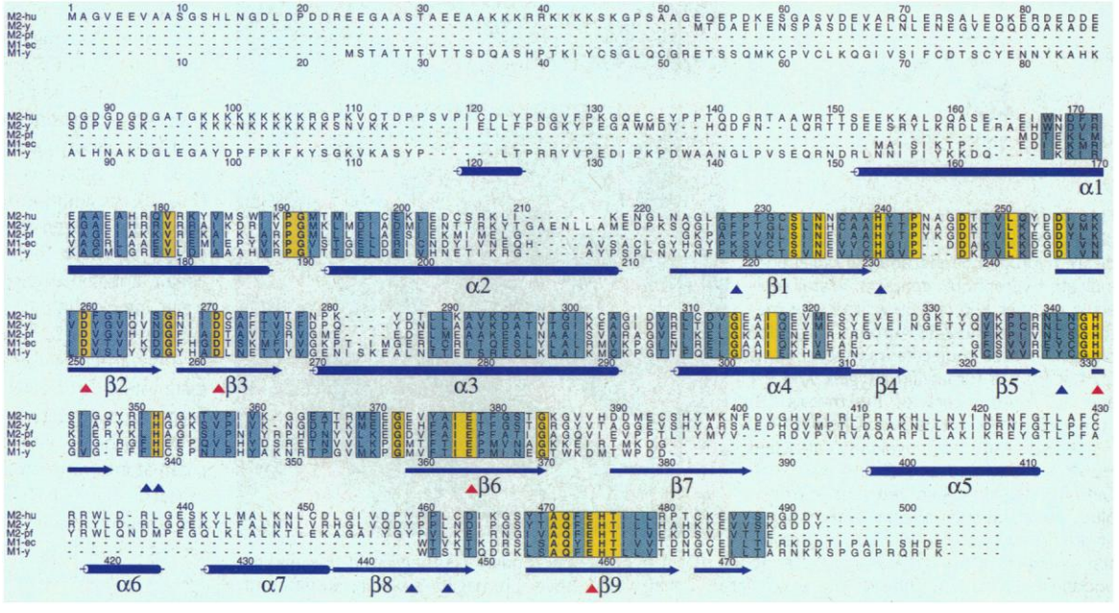

Fig. 2. Structure-based sequence alignment of selected MetAP sequences based on the three-dimensional structure of *E. coli* MetAP-1 (M1-ec) (*19*), *P. furiosus* MetAP-2 (M2-pf) (*20*), and human MetAP-2 (M2-hu). Numbers on top are sequence alignment numbers and those on the bottom are the sequence numbers of HsMetAP-2 used here. Yeast MetAP-1 (M1-y) and MetAP-2 (M2-y) sequences are from Swiss-Prot (ID numbers Q01662 and P38174, respectively). Similar and identical sequences are shaded by light blue and yellow, respectively. Red triangles are residues involved in metal coordination, and blue triangles are residues in contact with fumagillin. Figure prepared with Alscript (*17*).

MetAP-2 family and comes at the end of the long insertion that distinguishes the MetAP-2 family (Fig. 2). In the absence of fumagillin, the cobalts are coordinated by Asp^{251}, Asp^{262}, His^{331}, Glu^{364}, Glu^{459}, and a water molecule. The Asp^{262} and Glu^{459} residues are bidentate ligands coordinating both cobalts, Asp^{251} is bidentate with cobalt 1, Glu^{364} and His^{331} are monodentate with cobalt 2, and one clearly defined water molecule interacts with cobalt 2. All of the residues that coordinate the metals are on β strands near the center of the β sheet and are conserved in all MetAP sequences (Fig. 2).

The electron density for fumagillin was clearly visible in the difference electron density synthesis (Fig. 3A). Fumagillin has several structural components arrayed around its conformationally fixed cyclohexane ring, and a comparison of the active site of HsMetAP-2 with and without fumagillin shows how each component contributes to binding (Fig. 4, A and B). Earlier work had established that covalent bond formation causes fumagillin's irreversible inhibition, and the x-ray structure shows a covalent bond between an imidazole nitrogen (Nε2) atom of His^{231} and the carbon of the spirocyclic epoxide (*5*, *6*) (Fig. 3B). The formation of this C–N bond, although not predicted, is analogous to the alkylation of a catalytic histidine by α-chloroketone inhibitors of serine proteases (*14*). Histidine-231 does not move significantly upon bond formation; its nucleophilic imidazole nitrogen is perfectly positioned to bond with the methylene of the epoxide (Fig. 4B). The oxygen liberated from the breaking of the epoxide is coordinated with cobalt (3.28 Å), and it occupies the approximate position of the cobalt-associated water molecule in the uncomplexed structure. A water that is equidistant from both cobalts forms a hydrogen bond with this fumagillin oxygen (Fig. 4A). The only residue that moves significantly upon fumagillin complexation is His^{339}, which rotates its side chain to avoid close contacts with fumagillin (Fig. 4B).

The epoxide-bearing side chain of fumagillin occupies the completely covered pocket near the active site (Fig. 4B). It has hydrophobic contacts with His^{331} at the mouth of the pocket, Tyr^{444}, Ile^{338}, His^{339}, and Phe^{219} (Fig. 4B). A well-defined water molecule forms hydrogen bonds with the side chain epoxide and the methoxyl group at C5 (Fig. 4A). The long unsaturated side chain protrudes from the binding pocket and makes two hydrophobic contacts with Leu^{328} and Leu^{447}, and both residues are conserved in the MetAP-2 family (Figs. 3 and 4A). Leucine-447 lies near the end of the insertion that defines the MetAP-2 family, and the constriction formed by the Leu^{447}-Leu^{328} pair provides a structural basis for the MetAP-2 family's requirement for a substrate with a small (<1.3 Å radius of gyration) side chain at P2 (*15*). The terminal carboxyl of the side chain makes a hydrogen bond with Asp^{376}. Fumagillin can be analyzed as a substrate mimic with the epoxide-bearing side chain resembling methionine's side chain and the opened epoxide substituting for a nucleophilic water near the scissile carbonyl bond. The long unsaturated side chain protruding from the pocket mimics the COOH-terminal peptide chain.

The ability of fumagillin and related compounds to covalently inhibit MetAP-2 is even more remarkable in light of their specificity for MetAP-2 over MetAP-1 because the two enzymes have very similar active sites (Fig. 2). In yeast, either MetAP-1 or MetAP-2 function can be eliminated and the remaining enzyme will compensate (*16*). Elimination of both MetAP-1 and MetAP-2 function is lethal (*16*). Features that might generate such specificity can be highlighted by superimposing the 81 central core residues of HsMetAP-2 and EcMetAP-1 (0.83 Å root mean square deviation for main chain atoms) (Fig. 4C). In this superimposed model, $EcHis^{79}$, the residue that would covalently bond fumagillin, is too far away to form a bond. Two compensatory modifications are possible: moving fumagillin by about 1.6 Å toward $EcHis^{79}$ or moving $EcHis^{79}$ toward fumagillin. Moving fumagillin leads to severe steric clashes of C5 and the C6 methoxyl group with $EcTyr^{168}$ and of C7 and C8 with $EcCys^{78}$ (Fig. 4C). Tyrosine-168 is conserved in the MetAP-1 family, and its smaller counterpart, Leu^{328}, is conserved in the MetAP-2 family (Fig. 2). In addition to the steric clashes, the fumagillin oxygen that interacts with cobalt 2 would be more than 5 Å away from either cobalt, a distance greatly in excess of a metal-water interaction.

Moving $EcHis^{79}$ to bond with fumagillin also has troublesome features. The first is the assumption that $EcHis^{79}$ can be moved because its position appears to be fixed by a series of hydrogen bonds involving both main and side chain atoms between β1 and β2. The positions of $EcHis^{79}$ and $HsHis^{231}$ are also influenced by the adjacent residues, which are strongly conserved in both families: Ala-Ala-**His**-Tyr/Phe in MetAP-2 and Val/Ile-Cys-**His**-Gly in MetAP-1 (Fig. 2). If $EcHis^{79}$ could be moved to bond with fumagillin, there would be problems ac-

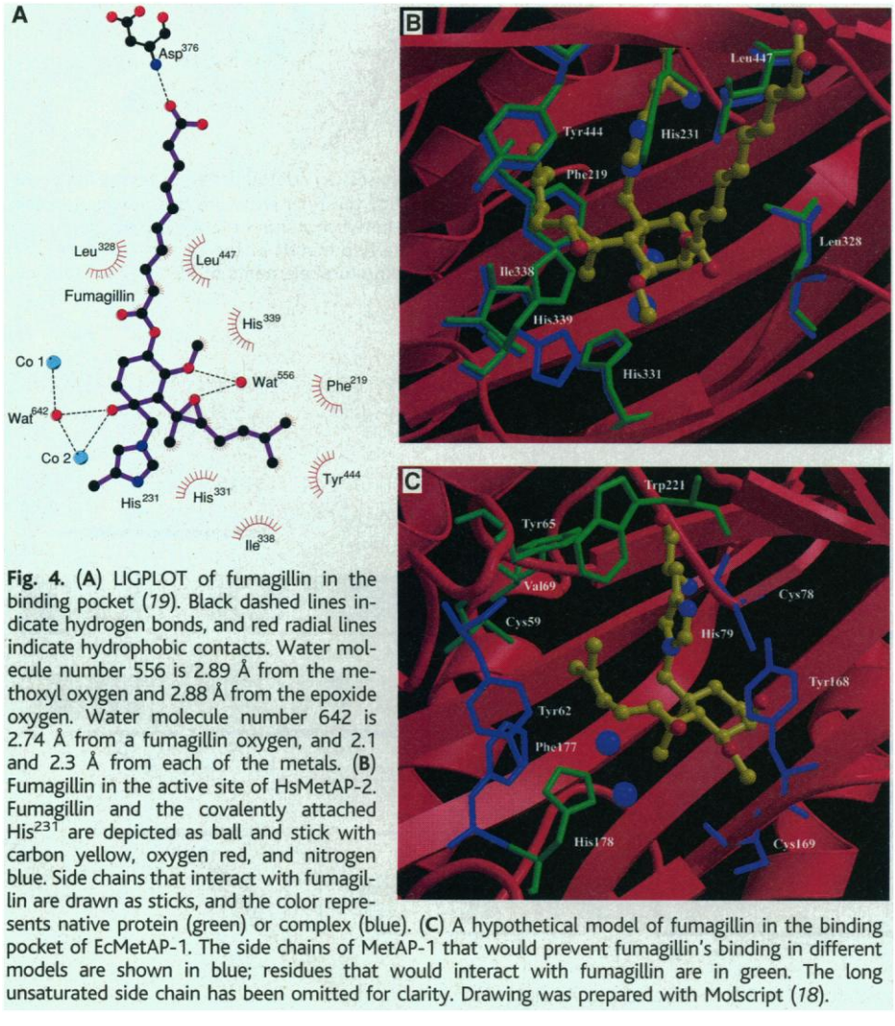

Fig. 4. (**A**) LIGPLOT of fumagillin in the binding pocket (*19*). Black dashed lines indicate hydrogen bonds, and red radial lines indicate hydrophobic contacts. Water molecule number 556 is 2.89 Å from the methoxyl oxygen and 2.88 Å from the epoxide oxygen. Water molecule number 642 is 2.74 Å from a fumagillin oxygen, and 2.1 and 2.3 Å from each of the metals. (**B**) Fumagillin in the active site of HsMetAP-2. Fumagillin and the covalently attached His^{231} are depicted as ball and stick with carbon yellow, oxygen red, and nitrogen blue. Side chains that interact with fumagillin are drawn as sticks, and the color represents native protein (green) or complex (blue). (**C**) A hypothetical model of fumagillin in the binding pocket of EcMetAP-1. The side chains of MetAP-1 that would prevent fumagillin's binding in different models are shown in blue; residues that would interact with fumagillin are in green. The long unsaturated side chain has been omitted for clarity. Drawing was prepared with Molscript (*18*).

commodating fumagillin's side chain in the specificity pocket. In MetAP-1, the size of the conserved Phe^{177} ($HsIle^{338}$) makes the pocket substantially narrower (Figs. 2 and 4C). The relatively slim side chain of methionine can be accommodated in this narrower pocket whereas the bulky and conformationally restricted side chain of fumagillin cannot. Because MetAP-1 lacks Tyr^{444} and has an open specificity pocket, the narrower pocket would be easily accessible. Thus, fumagillin's inability to inhibit MetAP-1 can be traced to the position of the nucleophilic His in MetAP-1, the difficulty of repositioning this residue because of consistent size differences in the adjacent residues, and a narrowing of the specificity pocket.

Our results provide a structural framework for understanding the relation of human MetAP-2 to prokaryotic and other eukaryotic MetAPs, fumagillin's ability to inhibit MetAP-2, and the basis of fumagillin's specificity. Insights from this analysis will also be useful in structure-based drug design. Fumagillin-based therapeutics such as TNP-470 share fumagillin's conformationally rigid template and key features. The two drugs differ in the side chain at C6, a region that shows few, if any, ligand interactions. Thus, TNP-470 is likely to inhibit MetAP-2 by occupying the active site in the same fashion as fumagillin.

References and Notes

1. J. Folkman, *Nature Med.* **1**, 27 (1995).
2. M. McCowen, M. Callender, J. F. Lawlis Jr., *Science* **113**, 202 (1951); F. R. Hanson and T. E. Eble, *J. Bacteriol.* **58**, 527 (1949).
3. D. Ingber *et al.*, *Nature* **348**, 555 (1990).
4. B. J. Dezube *et al.*, *J. Clin. Oncol.* **16**, 1444 (1998); Y. Kawarada *et al.*, *Pancreas* **15**, 251 (1997); H. Konno *et al.*, *Cancer* **77**, 1736 (1996); Y. Ohta *et al.*, *Br. J. Cancer* **75**, 512 (1997); Y. Singh *et al.*, *Breast Cancer Res. Treat.* **45**, 15 (1997); E. Wassberg and R. Christofferson, *Eur. J. Cancer* **33**, 2020 (1997); J. L. Xia *et al.*, *J. Cancer Res. Clin. Oncol.* **123**, 383 (1997); P. Twardowski and W. J. Gradishar, *Curr. Opin. Oncol.* **9**, 584 (1997).
5. N. Sin *et al.*, *Proc. Natl. Acad. Sci. U.S.A.* **94**, 6099 (1997).
6. E. C. Griffith *et al.*, *Chem. Biol.* **4**, 461 (1997).
7. J. Wang, N. Quan, J. Henkin, *Proc. Am. Assoc. Cancer Res.* **39**, 98 (abstr.) (1998).
8. S. M. Arfin *et al.*, *Proc. Natl. Acad. Sci. U.S.A.* **92**, 7714 (1995).
9. The entire HsMetAP-2 reading frame was excised from pBluescript and inserted into the pAcSG2 baculovirus transfer vector (Pharmingen, San Diego). This plasmid was cotransfected with BacVector-3000 (Novagen, Milwaukee, WI) into Sf9 cells. The virus was cloned and the protein expressed in Sf21 cells grown in Cyto-SF9 medium (Kemp Biotechnologies, Frederick, MD). A cell pellet from 2.5 liters of culture was lysed in 100 ml of 20 mM Hepes (pH 7.4), 150 mM NaCl, 10% glycerol, and protease inhibitors. The lysate was centrifuged at 48,000*g* for 1 hour, and two volumes of 10 mM Hepes (pH 7.4) were added to the supernatant. The material was applied to an SP-Sepharose (Pharmacia) column equilibrated with 10 mM Hepes. The column was washed with the Hepes containing 100 mM NaCl, and the proteins were eluted with a linear gradient from 100 to 500 mM NaCl in Hepes buffer. Fractions with MetAP-2 were combined and dialyzed against 100 mM potassium phosphate, pH 7.0, and applied to a hydroxylapatite (Bio-Rad, CHT type 1) column equilibrated with the same buffer. Proteins were eluted with a linear gradient from 100 to 400 mM potassium phosphate, pH 7.0. We obtained more than 20 mg of pure MetAP-2 per liter of culture. Mass spectroscopy gave a molecular weight of 53,060, and the NH_2-terminus appeared to be blocked. The protein was stored at 4°C in 10 mM Hepes, 10% glycerol, 150 mM NaCl, and 1 mM $CoCl_2$.
10. Crystals of HsMetAP-2 were grown in 1 to 2 weeks at 4°C from sitting drops, with a protein concentration of 12 mg/ml in 10 mM Hepes (pH 7.2), 10% glycerol, and 100 mM NaCl. The reservoir solution contained 15 to 30% *t*-butanol in 33 to 100 mM sodium citrate buffer, pH 5.2 to 5.6. The crystals belong to the orthorhombic space group $C222_1$ with a = 90.49 Å, b = 99.38 Å, and c = 101.59 Å and contain one molecule in the asymmetric unit. HsMetAP-2–fumagillin complex crystals were prepared by adding 1 μl of 50 mM fumagillin (ethanol) directly into a crystallization drop and equilibrated for 12 hours before mounting.
11. We collected data for both MetAP-2 and its fumagillin complex to a resolution of 1.8 Å (154,879 and 158,945 measurements of 42,194 and 40,944 unique reflections, 98.8% and 94.7% completeness, 3.7 and 3.9 redundancy, and R_{sym} values of 0.069 and 0.078, respectively) at the F1 station of CHESS (Cornell High-Energy Synchrotron Source) using 0.922 Å radiation ($R_{sym} = \Sigma\ |I - \langle I\rangle|/\Sigma\langle I\rangle$, where I is the integrated intensity of a given reflection). Phases were obtained by the molecular replacement technique as implemented in AMoRe [J. Navaza, *Acta Crystallogr. Sect. D Biol. Crystallogr.* **50**, 157 (1994)] and the 1.75 Å resolution model of PfMetAP-2 (*13*), Protein Data Bank accession code 1XGS. Extensive model building with O [T. A. Jones, J. Y. Zou, S. W. Cowan, M. Kjeldgaard, *Acta Crystallogr. Sect. A* **47**, 110 (1991)] and rigid body and restrained refinement with X-PLOR [A. T. Brünger, J. Kuriyan, M. Karplus, *Science* **235**, 458 (1987)] and REFMAC [G. N. Murshudov, A. A. Vagin, E. J. Dodson, *Acta Crystallogr. Sect. D Biol. Crystallogr.* **53**, 240 (1997)] brought the conventional R and R_{free} (calculated for 7% and 5% of the data not used for the refinement of native and complex, respectively) below 0.20 and 0.25, respectively. At this stage in the structure of the fumagillin complex, a fumagillin model could easily be built into the well-defined difference electron density map. The current models include 355 residues (110 through 138 and 153 through 478), two cobalt atoms, 240 waters, and two *t*-butanols for the native structure. In the complex structure, there are 203 waters, no *t*-butanols, and 33 fumagillin atoms. The current R values from 25.0 to 1.8 Å are 0.183 and 0.194 for the native and complex structures (0.228 and 0.231 for R_{free}). The root mean square deviations from ideal bond lengths and bond angles are 0.012 Å and 2.2°.
12. S. L. Roderick and B. W. Matthews, *Biochemistry* **32**, 3907 (1993).
13. T. H. Tahirov *et al.*, *J. Struct. Biol.* **121**, 68 (1998).
14. J. Kraut, *Annu. Rev. Biochem.* **46**, 331 (1977).
15. R. L. Kendall and R. A. Bradshaw, *J. Biol. Chem.* **267**, 20667 (1992).
16. X. Li and Y.-H. Chang, *Proc. Natl. Acad. Sci. U.S.A.* **92**, 12357 (1995).
17. G. J. Barton, *Protein Eng.* **6**, 37 (1993).
18. P. J. Kraulis, *J. Appl. Cryst.* **24**, 946 (1991).
19. A. C. Wallace, R. Laskowski, J. Thornton, *Protein Eng.* **8**, 127 (1995).

20. We thank R. Gillilan for graphics, the MacCHESS staff for help with data collection, J. Liu for helpful discussions, and Y.-H. Chang for the HsMetAP-2 pBluescript plasmid. The Cornell work was funded in part by U.S. Public Health Service grants CA59021 and CA24487 (to J.C.). C.M.C. is a Donaghue Foundation New Investigator. Atomic coordinates have been deposited in the Protein Data Bank under accession numbers 1BN5 (HsMetAP-2) and 1BOA (HsMetAP-2–fumagillin).

7 August 1998; accepted 7 October 1998

A Structural Explanation for the Recognition of Tyrosine-Based Endocytotic Signals

David J. Owen and Philip R. Evans*

Many cell surface proteins are marked for endocytosis by a cytoplasmic sequence motif, tyrosine-X-X-(hydrophobic residue), that is recognized by the μ2 subunit of AP2 adaptors. Crystal structures of the internalization signal binding domain of μ2 complexed with the internalization signal peptides of epidermal growth factor receptor and the trans-Golgi network protein TGN38 have been determined at 2.7 angstrom resolution. The signal peptides adopted an extended conformation rather than the expected tight turn. Specificity was conferred by hydrophobic pockets that bind the tyrosine and leucine in the peptide. In the crystal, the protein forms dimers that could increase the strength and specificity of binding to dimeric receptors.

The localization and movement of compartment-specific proteins within the cell is largely achieved through the recognition of short sequence motifs by targeting proteins. One of the most studied processes involving such signal recognition is clathrin-mediated endocytosis, which occurs in vesicle trafficking and the internalization of nutrient and growth factor receptors when bound to their appropriate cargo molecules [reviewed in (*1*)]. During the internalization of activated growth factor receptors such as the epidermal growth factor receptor (EGFR) tyrosine kinase [reviewed in (*2*)], receptors are removed from the cell surface in clathrin-coated vesicles and ultimately directed to the endosome and lysosome, where they are inactivated by proteolytic degradation (*3*, *4*).

Medical Research Council Laboratory of Molecular Biology, Hills Road, Cambridge CB2 2QH, UK.

*To whom correspondence should be addressed. E-mail: pre@mrc-lmb.cam.ac.uk